

Tunable site- and orbital-selective Mott transition and quantum confinement effects in $\text{La}_{0.5}\text{Ca}_{0.5}\text{MnO}_3$ nanoclusters

A. Valli^{1,2}, H. Das^{3,4}, G. Sangiovanni⁵, T. Saha-Dasgupta³, and K. Held¹

¹ *Institute for Solid State Physics, Vienna University of Technology, 1040 Wien, Austria*

² *Democritos National Simulation Center, CNR-IOM and Scuola Internazionale Superiore di Studi Avanzati (SISSA), 34136 Trieste, Italy*

³ *S.N. Bose National Centre for Basic Sciences, 700098 Kolkata, India*

⁴ *School of Applied and Engineering Physics, Cornell University, Ithaca, 14853 New York, USA*

⁵ *Institute for Theoretical Physics and Astrophysics, University of Würzburg, Am Hubland, 97074 Würzburg, Germany*

(Dated: June 16, 2021)

We present a dynamical mean-field theory (DMFT) study of the charge and orbital correlations in finite-size $\text{La}_{0.5}\text{Ca}_{0.5}\text{MnO}_3$ (LCMO) nanoclusters. Upon nanostructuring LCMO to clusters of 3 nm diameter, the size reduction induces an insulator-to-metal transition in the high-temperature paramagnetic phase. This is ascribed to the reduction in charge disproportionation between Mn sites with different nominal valence [Das *et al.*, Phys. Rev. Lett. **107**, 197202 (2011)]. Here we show that upon further reducing the system size to a few-atom nanoclusters, quantum confinement effects come into play. These lead to the opposite effect: the nanocluster turns insulating again and the charge disproportionation between Mn sites, as well as the orbital polarization, are enhanced. Electron doping by means of external gate voltage on few-atom nanoclusters is found to trigger a site- and orbital-selective Mott transition. Our results suggest that LCMO nanoclusters could be employed for the realization of technological devices, exploiting the proximity to the Mott transition and its control by size and gate voltage.

PACS numbers: 71.27.+a, 71.10.Fd, 71.30.+h, 75.47.Gk

I. INTRODUCTION

Research on manganites dates back to the 1950's, when Jonker and van Santen¹ reported the existence of ferromagnetic metallic phase in mixed crystals of manganese oxides $\text{LaMnO}_3\text{-CaMnO}_3$, $\text{LaMnO}_3\text{-SrMnO}_3$, and $\text{LaMnO}_3\text{-BaMnO}_3$. However, the interest of a wide portion of the scientific community was only raised in the 1990s, due to the experimental observation of a colossal magnetoresistance (CMR) effect.^{2,3} Indeed, the relative change in resistivity upon the application of an external magnetic field was much higher than the one observed in artificial magnetic/non-magnetic multilayer systems: up to 60% at room temperature in thin films.^{2,4} Triggering such a CMR, however, requires cooling below the Curie temperature T_C and the application of relatively strong magnetic fields, preventing the technical application of the CMR effect to this day. Alternative routes to achieve CMR have also been followed in mixed valence manganites such as the half-doped $\text{La}_{0.5}\text{Ca}_{0.5}\text{MnO}_3$ (LCMO),⁵ which is insulating below 155 K and displays antiferromagnetic and charge order,⁶ often also accompanied by orbital order. Indeed, the antiferromagnetic insulating state is prone to instabilities. The transition toward a ferromagnetic metallic state can be triggered upon applying a magnetic field,⁷ doping, biaxial strain, pressure,⁸ or an electric field.⁹ The experiments¹⁰⁻¹⁴ suggest that the destabilization of the charge-orbital order can also be obtained upon size reduction. In fact, it was observed also in $\text{Nd}_{1-x}\text{Ca}_x\text{MnO}_3$ ^{16,17} and $\text{Sm}_{1-x}\text{Ca}_x\text{MnO}_3$ ¹⁸ in both at half-doping and in asymmetrically doped samples, as

well as in $\text{Pr}_{0.5}\text{Ca}_{0.5}\text{MnO}_3$ ¹⁹⁻²¹ compounds. Nonetheless, there remains some controversy¹⁵ arising from the experimental difficulty to disentangle the effects of size reduction from other effects, such as oxygen non-stoichiometry, disorder, strain etc.

On the theoretical side, the effects of size reduction has been studied by density functional theory (DFT)+ U ²²⁻²⁴ and DFT+dynamical mean-field theory (DMFT).²² The theoretical analysis is in remarkable agreement with the experiments and shows a correlation-driven destabilization of the charge-orbital order in bulk LCMO upon size reduction. This bears the prospects that, for the optimized size, a much smaller magnetic field is sufficient to trigger a CMR, as LCMO nanoclusters can be tuned to the verge of a metal-insulator transition. Hitherto, the DFT+DMFT calculations on this topic, e.g., those reported in Ref. 22, were performed for bulk model systems with *ab-initio* parameters. That is, following the DFT calculations for 3 nm clusters, model bulk systems were constructed having the same unit cell volume as well as octahedral distortion as in the core of 3 nm cluster. This way, it was possible to take into account the interplay between strong electronic correlations within DMFT and the structural distortions induced by size reduction, obtained *ab-initio* through atomic relaxation within DFT. In this paper, we take a significant step forward, in terms of carrying out nanoscopic DMFT calculations for few-atom clusters with a DFT-derived tight-binding Hamiltonian. This gives us the opportunity to consider the effect of size reduction from bulk to intermediate-sized clusters to few-atom clusters. Our calculations show an interesting evolution from the high-temperature param-

agnetic insulating (PI) state in the bulk to a paramagnetic metallic (PM) state in intermediate-sized clusters to re-entrant insulating solution for few-atom clusters. We also investigate the effects of applied hydrostatic pressure in the bulk, which turn out to be different than the effects of size reduction. Considering few-atom clusters, we also show that electron doping, through the application of external gate voltage, drives an unexpected site- and orbital-selective Mott transition.

The paper is organized as following. In Section II we discuss the model employed for the description of mixed-valence manganites, and we describe the strategy we followed to include structural, finite-size, and many-body effects in the framework of a combined DFT+DMFT approach. In Sec. III we present the DMFT results obtained for LCMO nanoclusters of different size. In particular, in Sec. III A we focus on the effects of quantum confinement on the spectral properties, while in Sec. III B we explore the effect of electrostatic doping by applying an external gate voltage to the few-atom clusters. Finally, in Sec. IV we present our conclusions.

II. METHOD: DFT+DMFT APPROACH FOR $\text{LA}_{0.5}\text{CA}_{0.5}\text{MNO}_3$ NANOCCLUSERS

A. Bulk crystal and electronic structure

Manganites, $\text{R}_{1-x}\text{A}_x\text{MnO}_3$ with R being a trivalent rare-earth-metal element and A a divalent dopant, have a perovskite lattice structure, with the rare-earth atoms at corner positions, the Mn atoms at body center positions and oxygen atoms at the face centered positions. Depending on the sizes of R and A, given by the so-called tolerance factor, the MnO_6 octahedra can tilt and rotate reducing the symmetry of the perovskite lattice from cubic to orthorhombic. With nominal oxygen valency O^{2-} , in half-doped compounds (i.e., $x = 0.5$) the manganite atoms are in a mixed valent $\text{Mn}^{3.5+}$ state. This can lead to a charge disproportionation between the Mn sites in bulk half-doped manganites; in the extreme case one has a 50% of Mn^{4+} sites with a $3d^3$ configuration, and the other 50% of Mn^{3+} sites with a $3d^4$ configuration. The charge-ordered state is associated with a real space ordering of $\text{Mn}^{3+}/\text{Mn}^{4+}$ species in a 1:1 pattern. The octahedral crystal field surrounding the Mn ions splits the $3d$ orbitals into three low energy t_{2g} orbitals (d_{xy} , d_{xz} , and d_{yz}) and two higher energy e_g orbitals ($d_{3z^2-r^2}$ and $d_{x^2-y^2}$). Due to the strong Hund's exchange coupling, the three Mn electrons of Mn^{4+} occupy the t_{2g} orbital, in a high-spin $S_{t_{2g}} = 3/2$ configuration. The consequent energy gain associated to this state, makes it energetically favorable for the extra electron of Mn^{3+} to occupy the doubly degenerate e_g states. Hence, the charge ordering accommodates a static Jahn-Teller distortion at the Mn^{3+} sites, removing the degeneracy and lowering the symmetry of the system to monoclinic.

The Mn e_g orbitals are delocalized due to a strong

hybridization with the $\text{O}2p$ states. On the contrary, Mn t_{2g} orbitals do not hybridize strongly with the O and are localized. The magnetism is thus governed by the double exchange mechanism.²⁵

B. DFT calculations and downfolding procedure

The first step of our study is a DFT calculation of both LCMO bulk and nanoclusters. To this end, we use projected augmented wave (PAW) pseudopotentials with an energy cutoff of 450 eV and performed calculations within a spin-polarized generalized gradient approximation (GGA)²⁶ as implemented in the Vienna *ab-initio* Simulation Package (VASP).²⁷⁻³⁰ The forces on the atoms are converged to less than 0.01 eV/Å. All DFT calculations for bulk LCMO was performed with a $4 \times 2 \times 4$ k -mesh. On the other hand, for the nanoclusters we use only the Γ point for the k -space integration. The structural optimization of the bulk LCMO is performed considering both antiferromagnetic (AFM) CE and ferromagnetic (FM) configurations. We find the AFM CE phase to be lower in energy compared to the FM phase by 45 meV/f.u. The stoichiometry of the system is maintained in the construction of the nano-clusters, as discussed in Refs. 22 and 23.

A necessary step for the subsequent DMFT calculation is the extraction of the relevant tight-binding parameters, calculated *ab initio* within DFT. To achieve this, we employ the downfolding method as implemented in the N-th order muffin tin orbital (NMTO) basis^{31,32} with potential parameters borrowed from self-consistent linearized muffin-tin orbital (LMTO)³¹ calculations. Through the NMTO-downfolding procedure, a low-energy Hamiltonian $H(k)$ involving only Mn e_g Wannier orbitals³³ is constructed in k -space by integrating out all other degrees of freedom. The Fourier transformation of $H(k)$ provides the tight-binding parameters. In the following we refer to this structure as S_{bulk} . We use S_{bulk} to describe bulk manganites within standard DFT+DMFT calculations. In order to construct a low-energy Hamiltonian for the nanoclusters, as explained in Ref. 22, a cluster of nearly spherical shape having 3 nm diameter is cut out from a large supercell of the bulk crystal structure in monoclinic $\text{P}2_1/\text{m}$ symmetry, which is then subject to a full structural optimization. In the following we refer to this structure as S_{nano} . The NMTO-downfolding calculation is then carried out on the self-consistent LMTO calculation for a model bulk structure, referred to as S_{model} , which is constructed considering the MnO_6 octahedra selected from the core region of S_{nano} , and applying various symmetry operations, as explained in detail in Ref. 23. The DF-derived tight-binding Hamiltonians contain the information of the structural as well as electronic changes at the level of one-electron theory that happen upon size reduction.

In order to take into account many-body effects within DMFT, we build a low-energy model (discussed in detail

in Sec. II C) with the DFT-derived hopping parameters as an input. However, there is fundamental difference between the calculations performed in this work and that of Ref. 22, as explained is the following: In Ref. 22, we performed DMFT calculations on the constructed model *bulk* structure (S_{model}). Instead, in the present work, we use the same parameters of S_{model} to construct few/atom nanoclusters of different size, which we solve within the nano-DMFT scheme discussed in Sec. II D.

C. Low-energy effective $e_g + S_{t_{2g}}$ model

The low-energy Hamiltonian describing the manganites is given as below,^{34–36}

$$\begin{aligned} \mathcal{H} = & \sum_{ijmm'} \sum_{\sigma\sigma'} h_{ij,mm'} c_{im\sigma}^\dagger c_{jm'\sigma'} - \mathcal{J} S \sum_{im} (n_{im\uparrow} - n_{im\downarrow}) \\ & + U \sum_{im} n_{im\uparrow} n_{im\downarrow} + \sum_{imm'} \sum_{\sigma\sigma'} (U' - J\delta_{\sigma\sigma'}) n_{im\sigma} n_{im'\sigma'}. \end{aligned} \quad (1)$$

Here, $h_{ij,mm'}$ denotes the generic matrix element of the one-particle DFT Hamiltonian in the basis of the the downfolded NMTO Wannier orbitals m, m' at site i, j ; the on-site Coulomb interaction between the e_g electrons is parametrized in terms of an intra-orbital repulsion $U = 5$ eV, a Hund's exchange $J = 0.75$ eV, and an inter-orbital interaction $U' = U - 2J$.^{37,38} The values of the interaction parameters, taken from the literature,³⁹ represent realistic estimates for manganites. Furthermore, the e_g orbitals are coupled to a (classical) disordered spin S by a Hund's exchange \mathcal{J} . This term represents the interaction between the itinerant e_g electrons with the localized electrons in the half-filled t_{2g} manifold. In the notation adopted here, $S = \pm 1$ is the classical spin corresponding to the high-spin states of $S_{t_{2g}} = \pm 3/2$ while its modulus is included in the value $\mathcal{J} = 1.35$ eV.³⁶ Hamiltonian (1) represents a standard low-energy model for the description of electronic correlations in manganite compounds^{34–36} Recently, the classical spin description of the t_{2g} manifold has been thoroughly revisited.⁴⁰ Thanks to the significant technical improvements in the field of impurity solvers, this allows the direct treatment of a five-orbital model for the whole Mn3d multiplet, including also spin-flip and pair-hopping terms beyond the density-density Coulomb interaction.^{41,42} Remarkably, in the case of pure LaMnO₃, a detailed analysis showed an excellent agreement between a classical spin and a full quantum many-body treatment of the t_{2g} orbitals, e.g., for the e_g spectral functions.⁴⁰ Moreover, the estimate obtained for the spin-spin correlations functions $\langle S_z^{e_g} S_z^{t_{2g}} \rangle \approx 0.74$ was found to be consistent with the picture of aligned e_g and $S = 3/2$ t_{2g} spins.⁴⁰ In light of these considerations, the restriction to the low-energy model described by Hamiltonian (1) represents a realistic and physically sensible choice to study correlation effects in

Mn compounds with a half-filled t_{2g} manifold and partially filled e_g orbitals.

D. Dynamical mean-field theory with inequivalent Mn atoms in the unit cell

In the following we discuss the technical details for the solution of the many-body Hamiltonian (1) in the framework of DMFT^{38,43} for inhomogeneous systems.^{44–49} That is, we solve an auxiliary Anderson impurity problem for each inequivalent Mn site in the unit cell. Moreover, we perform an average over the disordered classical t_{2g} spin S .⁵⁰ This procedure yields a local 2×2 self-energy in the e_g manifold of each of the Mn atoms in the unit cell, while neglecting non-local self-energy elements between different Mn atoms. Let us start by discussing the bulk DFT+DMFT calculations, which have been performed on S_{bulk} and S_{model} structures to describe LCMO bulk and nanoscopic (3 nm) clusters. The bulk monoclinic unit cell of LCMO contains eight Mn atoms but only three kinds of Mn atoms are locally inequivalent, labeled as Mn1(1), Mn1(2), and Mn2. The four Mn1 atoms have a nominal valence 3+ and occupy the bridge sites of the zig-zag ferromagnetic chain in the CE-type magnetic order that sets in below the Néel temperature in bulk LCMO. Those Mn1 are further divided into two Mn1(1) and two Mn1(2) sites, by symmetry. The four Mn2 atoms have a nominal valence 4+ and occupy the corner sites of the zig-zag ferromagnetic chain. Exploiting these symmetries, the overall computational effort for the bulk amounts to the solution of three auxiliary impurity problems within a DMFT self-consistent scheme, with the corresponding subtraction of three inequivalent double counting terms in $h_{ij,mm'}$:

$$\Delta_{im}^{DC} = \tilde{U} \left(n_{im}^{\text{DFT}} - \frac{1}{2} \right), \quad (2)$$

where $\tilde{U} = U - \frac{5}{3}J$ denotes an averaged interaction and n_{im}^{DFT} are the NMTO orbital occupancies for each of the inequivalent Mn in the unit cell.^{38,52,53} In the numerical calculations, we employ a Hirsch-Fye Quantum Monte Carlo⁵⁴ impurity solver, with a Trotter discretization $\Delta\tau^2 \approx 0.027$ and inverse temperature $\beta = 20$ eV⁻¹ in the paramagnetic phase.

For the nano-DMFT calculations, we consider the LCMO finite-size nanoclusters shown in Fig. 1 and described by the structure S_{nano} . The symmetry of the nanoclusters is much lower than in the bulk due to finite-size effects. This leads to many more inequivalent Mn. For example, the $N = 46$ Mn atom cluster contains $N_{\text{ineq}} = 23$ inequivalent Mn sites, as it possesses only the inversion symmetry with respect to the center of the cluster. In this case, we need to solve for N_{ineq} impurity problems, yielding $N_{\text{ineq}} 2 \times 2$ local self-energy matrices $\Sigma_{mm'}^{ii}$. From these, new $(N \times 2) \times (N \times 2)$ cluster Green's functions are calculated by solving the Dyson equation, enforcing the self-consistency at the level of

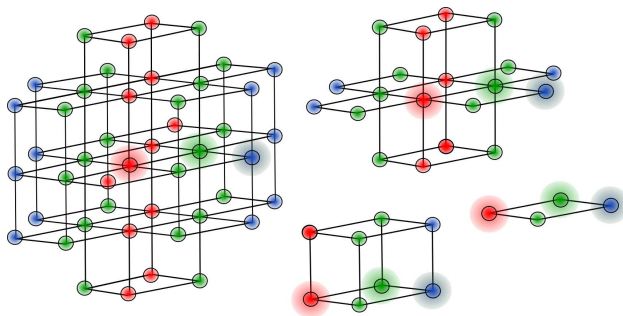


FIG. 1: (Color online) Schematic representation of the Mn sublattice of the few atom sized small clusters considered in the present DMFT work, having $N = 46, 20, 8,$ and 4 Mn sites. The clusters are built by chopping off atoms from the supercell described by the tight-binding Hamiltonian of S_{nano} . The red (gray), blue (dark gray) and green (light gray) atoms correspond to Mn1(1), Mn1(2), and Mn2, respectively, according to their classification in the bulk. The cluster boundaries correspond to dangling Mn-Mn bonds. La, Ca, and O atoms (not shown) are effectively taken into account in the *ab-initio* parameters of S_{nano} through the downfolding procedure.

the whole nanocluster. This scheme has been employed for all the few-atom Mn clusters, shown in Fig. 1, taking into account the specific symmetries of each structure. We stress once more that this nano-DMFT approach is different in spirit from that adopted in Ref. 22, in which bulk-DMFT calculations were performed, and the effect of size reduction was considered via the change in tight-binding parameters of S_{model} with respect to S_{bulk} . Instead, within nano-DMFT calculations we explicitly take into account the boundary effects of the finite-size nanoclusters constructed with the tight-binding parameters extracted from S_{nano} .

III. RESULTS FOR FINITE SIZE LCMO NANOCLUSTERS

A. Spectral properties, charge and orbital order

In the following we discuss the spectral properties of the nano clusters shown in Fig. 1. The DMFT spectral functions are shown in Figs. 2, for three representative Mn atoms belonging to Mn1(1), Mn1(2) and Mn2 kinds, following the bulk classification (even though for the nanoclusters the atoms of e.g. Mn1(1) type are of course not equivalent any longer as in S_{model}). At the outset, we notice that the size reduction has profound consequences on the electronic structure of the LCMO nanoclusters, in the sense that the metallic character decreases gradually in moving from $N = 46$ to 4 . In the extreme case of $N = 4$, the system is insulating even at the high temperature considered here ($\beta = 20 \text{ eV}^{-1}$), reflecting the strong quantum confinement effects induced upon size reduction. The observed metal-to-insulator transition is accompanied by a strong enhancement of the charge dis-

proportionation between Mn^{4+} and Mn^{3+} . We further find that size effects are accompanied by an overall enhancement of the orbital polarization. These effects are strong for Mn1(1) and Mn2 atoms which are located at the core of the clusters. Instead, all Mn1(2) sites are located at the surface of the clusters (with maximum number of dangling bonds) and have a nearly insulating and almost fully orbitally-polarized spectral function irrespective of cluster size.

In the bulk LCMO, the orbital polarization between two e_g orbitals, $3z^2 - r^2$ and $x^2 - y^2$ is complete for Mn1 atoms with nominal $3+$ valence, and zero for Mn2 atoms with nominal $4+$ valence. Moving to cluster of 3 nm diameter it was shown²² that both charge disproportionation between Mn1 and Mn2 atoms, as well as the orbital polarization at the Mn1 atoms decreases considerably compared to the bulk, leading to metallicity. Indeed, we find that upon further reduction of the size to few-atom nanoclusters, quantum confinement effect comes into play, making the charge disproportionation and orbital polarization increase again, especially for Mn1(1) atoms. Both charge disproportionation and orbital polarization show an increasing trend upon decreasing the cluster size, from $N = 46$ to 20 to 8 until it becomes almost complete for the $N = 4$ nanocluster.

In order to study quantitatively the effects of size reduction, we consider the cluster averaged charge order and the orbital polarization. To this end, we define the occupation n_i and the polarization p_i of Mn site i as

$$\begin{aligned} n_i &= \frac{1}{2} \sum_{\{S\}} \sum_{m\sigma} n_{im\sigma}^S, \\ p_i &= \frac{1}{2} \sum_{\{S\}} \sum_{m\sigma} n_{im\sigma}^S (-1)^m, \end{aligned} \quad (3)$$

where the average over $\{S\}$ takes into account the two possible configurations of the classical t_{2g} spin S (as discussed in Sec. II D). Hence, using the definitions above, we compute the following quantities

$$\begin{aligned} \langle \Delta n \rangle &= \frac{1}{N_\alpha} \sum_{i \in \alpha} n_i - \frac{1}{N_\beta} \sum_{i \in \beta} n_i, \\ \langle \Delta p_\alpha \rangle &= \frac{1}{N_\alpha} \sum_{i \in \alpha} p_i, \end{aligned} \quad (4)$$

where $\alpha \neq \beta$ denotes Mn1 and Mn2 sites, respectively, while N_α, N_β denote the number of Mn sites of the corresponding kind in the nanocluster. In particular, $\langle \Delta n \rangle$ is the charge disproportionation averaged over the nanocluster, while $\langle \Delta p_\alpha \rangle$ is the orbital polarization averaged over all Mn site in the nanocluster belonging to the same kind α . Note that in Eq. (4), the occupation n_i and the polarization p_i for the different Mn sites i (even those belonging to the same Mn kind α) are in general inequivalent because of the symmetry of the finite nanoclusters constructed from S_{nano} , which are different from the bulk models described by S_{bulk} or S_{model} .

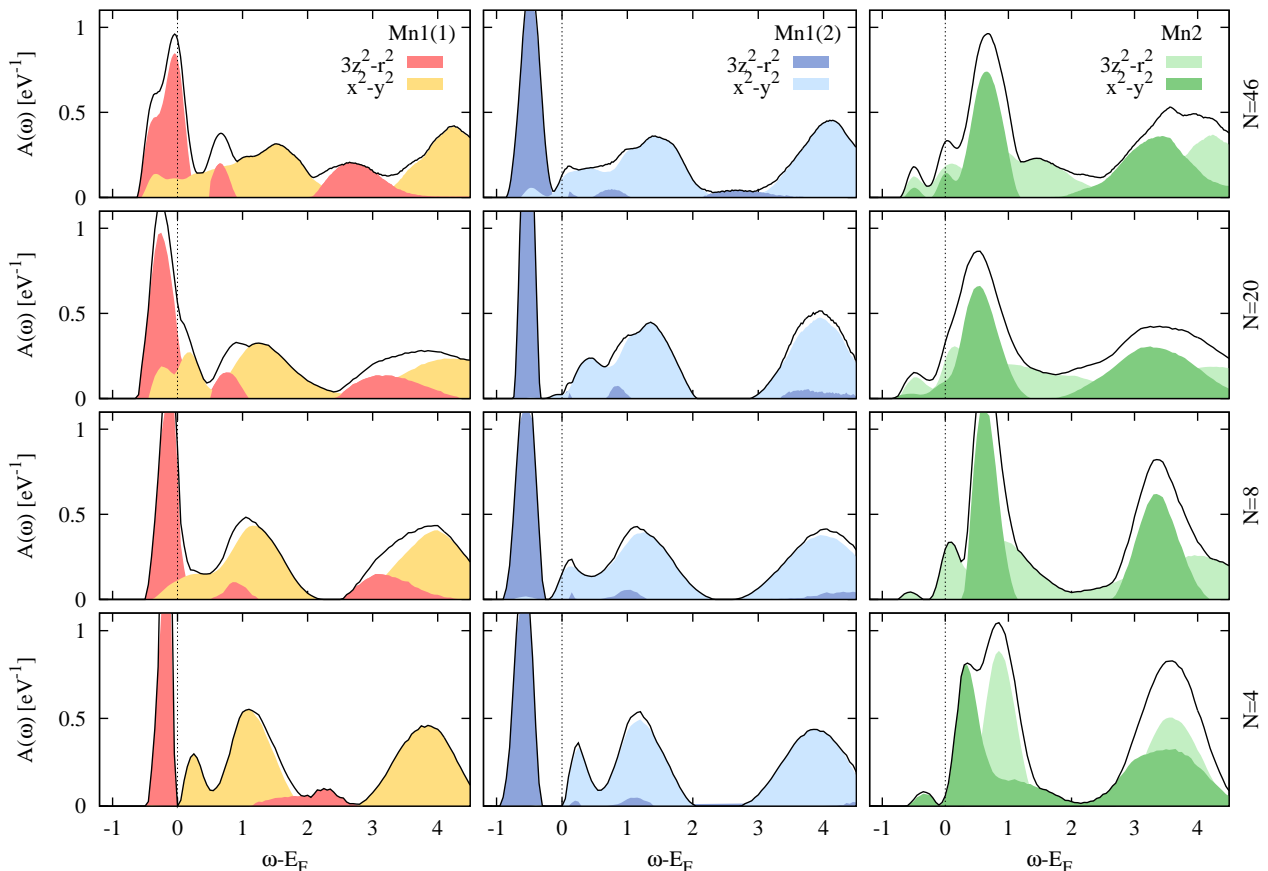


FIG. 2: (Color online) Evolution of the spectral properties of the nanoclusters, shown in Fig. 1, described by the tight-binding parameters of S_{nano} . Each row shows the spectral function $A(\omega)$ for a cluster having N Mn atoms. The red (gray), blue (dark gray) and green (light gray) lines correspond to representative Mn1(1), Mn1(2), and Mn2 atoms, respectively, indicated by shaded spheres in the nanoclusters shown in Fig. 1. The dark and light filled curves in each panel denote the contributions from the $3z^2 - r^2$ and $x^2 - y^2$ orbitals, while the black solid line denotes the on-site spectral density of the e_g manifold. A metal-to-insulator transition (MIT) upon decreasing cluster size, due to quantum confinement effect, is evidenced accompanied by an enhancement of the charge and orbital order.

The cluster-averaged $\langle \Delta n \rangle$ and $\langle \Delta p_\alpha \rangle$ are shown in the right-hand side of each panels in Fig. 3 as a function of the (inverse) number of the Mn atoms in the cluster. For comparison, on the left-hand side of each panel the results obtained in Ref. 22 within DFT+DMFT calculation performed on the bulk nanomodel S_{model} are also shown (applicable to 3 nm diameter cluster containing about 200 Mn atoms). As a general trend, the charge order and orbital polarization are found to be the largest for the smallest cluster and decrease upon increasing the cluster size. In particular, Δn shows a smooth reduction with increasing system size from a value close to $\Delta n = 1$ for $N = 4$, corresponding to the limit in which the Mn2 sites are completely empty, to $\Delta n \approx 0.70$ for $N = 46$. Those values can be compared to $\Delta n \approx 0.35$ found for the S_{nano} model. A similar behavior is found for the averaged orbital polarization, although the behavior is somewhat dependent on the system shape and symmetry, especially for the smaller nanoclusters consid-

ered here. However, in general the orbital polarization of the Mn1 atoms tends to decrease, by increasing cluster size, while that for the (almost empty) Mn2 atoms is always negligible. A more careful analysis (not shown) reveals that the averaged Δp is systematically larger than the one of the core Mn atoms (especially for larger clusters), as it also includes the contribution of Mn atoms on the surface of the cluster, which are characterized by sharper spectral structures and a stronger orbital polarization.

If we also consider the results obtained from the DFT+DMFT calculations of Ref. 22, we find that both the charge order $\langle \Delta n \rangle$ and the orbital polarization $\langle \Delta p_\alpha \rangle$ are strongly enhanced for S_{bulk} with respect to the 3 nm cluster size described by S_{model} , which drives a metal-to-insulator transition.²²

The above observations are depicted by the following scenario: Starting from the smallest size cluster and upon progressively increasing the system size, one encounters

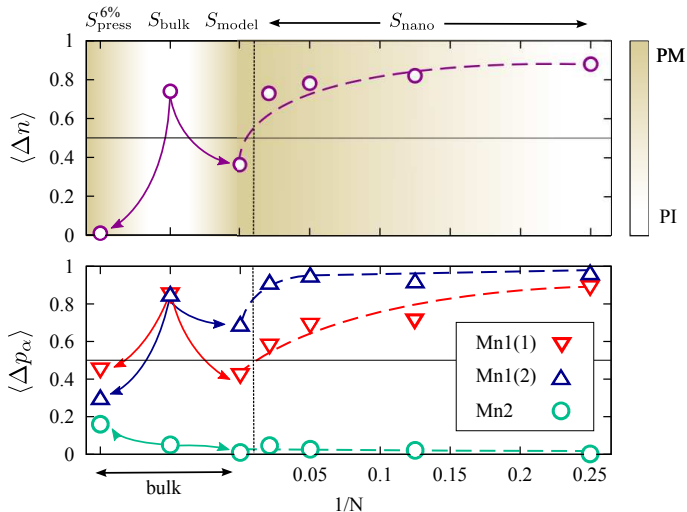


FIG. 3: (Color online) Cluster averaged charge order $\langle \Delta n \rangle$ (upper panel) and orbital polarization $\langle \Delta p_\alpha \rangle$ (lower panel) of LCMO bulk and clusters. On the right-hand side of each panes we show the nano-DMFT results obtained for the finite-size clusters built with the parameters of S_{nano} , as a function of the (inverse) number of the Mn atoms in the cluster. On the left-hand side of each panel we also show the DFT+DMFT results obtained within the calculations of Ref. 22 for the bulk model S_{model} (applicable for 3 nm diameter cluster containing about 200 Mn atoms) and on bulk LCMO S_{bulk} . Those are compared to additional DFT+DMFT result for S_{press} , corresponding to the bulk under the application of hydrostatic pressure, resulting into 6% volume reduction. The light brown (light tray) shade in the upper panel represents the transitions between PI and PM phases. Arrows and dashed lines are a guide to the eye.

TABLE I: Orbital DFT+DMFT occupancies for the three inequivalent Mn atoms in the unit cell of S_{model} and S_{press} . In brackets we give the corresponding occupancies for the one-particle low-energy DFT Hamiltonian without the effect of DMFT correlations, which strongly enhance the charge-orbital order. Both the orbital polarization in Mn1 atoms, as well as the charge disproportionation between Mn1 and Mn2 atoms are more pronounced for the nano model S_{model} than for the pressurized bulk system S_{press} .

| | Pressure 6% | | Nano model | |
|--------|--------------|-------------|--------------|-------------|
| | $3z^2 - r^2$ | $x^2 - y^2$ | $3z^2 - r^2$ | $x^2 - y^2$ |
| Mn1(1) | 0.52 (0.39) | 0.06 (0.11) | 0.52 (0.31) | 0.09 (0.20) |
| Mn1(2) | 0.36 (0.34) | 0.07 (0.13) | 0.72 (0.38) | 0.04 (0.19) |
| Mn2 | 0.33 (0.31) | 0.17 (0.21) | 0.16 (0.21) | 0.16 (0.25) |

an insulator-to-metal transition in few-atoms nanoclusters, which is driven by a weakening of quantum confinement effects and charge-orbital correlations. With increasing system size, the nanocluster smoothly evolves towards the results obtained with the bulk nanomodel, which is metallic due to the weak structural distortions included in the parameters of S_{model} . On the other hand,

bulk LCMO S_{bulk} is strongly distorted. The structural distortions lead to the enhancement of charge-orbital order and drive the system across a second metal-to-insulator transition between S_{model} (3 nm) and S_{bulk} (bulk).²²

It is interesting to compare the results obtained for S_{model} and for the bulk under applied hydrostatic pressure S_{press} corresponding to the same volume reduction of the unit cell, i.e., 6% for 3 nm nanocluster described by S_{model} . We find that the effects of hydrostatic pressure and the size reduction are rather different. The results for S_{press} indicate that charge order and orbital polarization are strongly reduced with respect to the case of S_{model} , as shown in detail in Table I. In particular, we find that for S_{press} the charge disproportionation between Mn^{3+} and Mn^{4+} is negligible, and it is accompanied by an overall reduction of the orbital polarization. This makes the system under hydrostatic pressure to be far more metallic compared to a 3 nm cluster.

B. Site- and orbital-selective Mott transition driven by applied gate voltage

The interesting insulator-to-metal-to-insulator transition in LCMO upon size reduction is based on a complex interplay between quantum confinement effects and the structural distortions occurring upon size reduction from the bulk LCMO to 3 nm nanoclusters. As the onset of the peculiar charge- and orbital-ordered state found in the bulk LCMO relies on the balance between Mn^{3+} and Mn^{4+} , it is interesting to study the effect of electron doping on the few-atom clusters. A change in the number of carriers without changing the chemical composition of the system can be achieved by the application of an external gate voltage V_g . In this section, we investigate this issue through DMFT calculations considering the clusters with $N = 46$ and 4 Mn atoms. We consider the limiting case where there is only an infinitesimally small tunneling contact with the environment, so that we can account for the gate voltage by changing the DMFT chemical potential. We neglect the effect of doping on the DFT effective potential, as in the virtual crystal approximation.⁵⁵ In Fig. 4 we show the orbitally-resolved spectral weight at the Fermi energy $A(E_F)$ (averaged over a unite energy window $\sim T$) as calculated from the Green function at imaginary time $\tau = \beta/2$, and the occupancies of the two e_g orbitals for representative sites of S_{nano} with $N = 46$ and $N = 4$ Mn sites clusters. The value $V_g = 0$ corresponds to the results in the previous sections and to an average cluster occupation $\langle n \rangle = 0.5$ electrons in the e_g orbitals. Upon changing V_g , we increase the number electrons in the LCMO cluster (electron doping). When the low-lying e_g orbital (e.g., the $x^2 - y^2$ in the case of Mn1) on a Mn site becomes half-filled, strong electronic correlations drive an orbital-selective metal-to-insulator transition, with the opening of a Mott gap. Such an orbital-selective Mott transition has been reported before for the

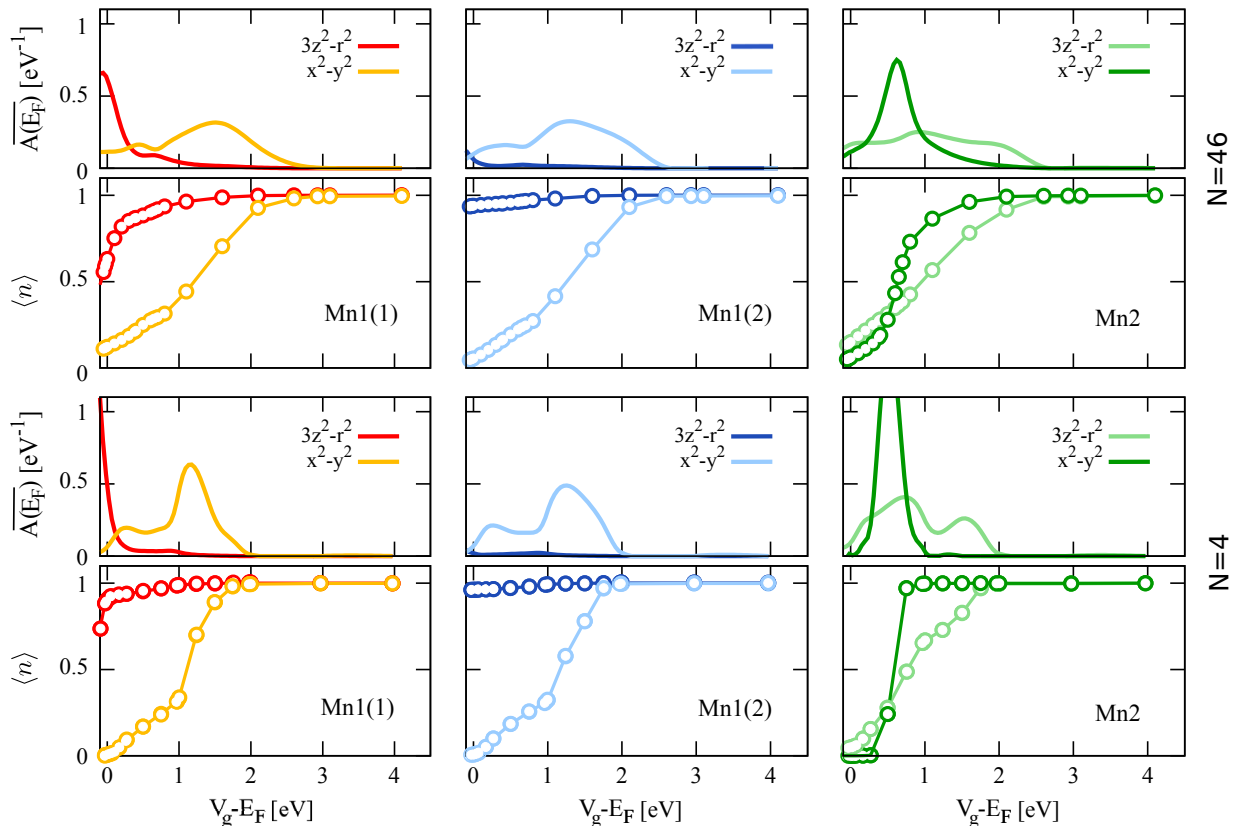


FIG. 4: (Color online) Evolution of the spectral weight at the Fermi energy $\overline{A(E_F)}$ (averaged over a unite energy window $\sim T$) and of the orbitally-resolved occupation with gate voltage V_g (electron doping) for the representative Mn sites of the $N = 46$ (upper panels) and $N = 4$ (lower panels) clusters. The red (gray) blue (dark gray) and green (light gray) curves correspond to representative Mn1(1), Mn1(2), and Mn2 atoms, respectively, while the light and dark colors denote $3z^2 - r^2$ and $x^2 - y^2$ states. The gate voltage V_g drives an orbital selective Mott transition, which becomes sharper upon decreasing the system size.

Hubbard model, originating from different bandwidth (or correlations) for different orbitals,^{56–61} or due to the band degeneracy lifting,⁶² as well as for materials.^{63–65} The charge disproportionation between Mn^{3+} and Mn^{4+} also results in a strong site-selective character of the transition. Site-selective behavior of similar kind has also been reported recently for bulk systems^{66,67}. In our case, we have one insulating orbital which is integer filled ($n = 1$), but neither the occupation of the other (metallic) orbital, nor the cluster average electron density is integer. One possible interpretation of this novel orbital- and site-selective Mott transition is associated to the role of the Hund's exchange coupling to the t_{2g} -spins. A filling of one electron in an orbital thus means that all states with spin parallel to the t_{2g} -spins are occupied, while those with opposite spin are empty.

The orbital-selective MIT is relatively homogeneous in the cluster, meaning that e_g Mn sites of the same kind turn insulating at a similar value of V_g . On the other hand, the critical value of V_g still depends both on the kind of Mn site and the cluster size. Further increasing V_g increases the population of the other e_g orbital (e.g., the $3z^2 - r^2$ in the case of Mn1). Above $V_g \approx 2.6$ eV (until the chemical potential lies within the Mott gap) all orbitals

are half-filled and Mott insulating, with $A(E_F) = 0$ (see upper panels in Fig. 4) and display a divergent imaginary part of the DMFT self-energy (not shown). In general, we observe that, upon decreasing the cluster size, the orbital-selective MIT is found at a smaller value of V_g . The transition also appears to be sharper upon changing V_g . This can be understood by considering the more localized nature of the e_g orbitals and the enhanced orbital polarization observed for smaller cluster sizes. This effect is important in view of possible applications. For an appropriate system size, half-doped LCMO nanocluster can be driven across a MIT by applying an external gate voltage.

IV. CONCLUSIONS

We investigated the effects of size reduction on the charge and orbital order in the LCMO mixed valence manganite within the DFT+DMFT framework. As was shown before,²² the size reduction from bulk to a 3 nm nanoclusters weaken the distortions the bulk crystal structure and induces an insulator(bulk)-to-metal(3 nm)

transition in the high-temperature paramagnetic phase, along with a weakening of charge and orbital disproportionation. Here, we extend the analysis by considering nanoclusters of just a few-atoms. Upon reducing the system size we observe the opposite trend: driven by the quantum confinement, there is a second metal(3 nm)-to-insulator(few atoms) transition and an enhancement of both charge and orbital disproportionation. We also investigated the effect of electron doping on the few-atom nanoclusters by applying an external gate voltage. We observe an orbital-selective Mott transition at a critical value of the gate voltage which corresponds to an integer filling of only an individual e_g orbital. The orbital-selective nature of the transition is a direct consequence of the orbital polarization and the strong Hund's exchange splitting. At the same time, the strong charge disproportionation between Mn^{3+} and Mn^{4+} sites induces also a site-selective character, with different Mn kinds turning insulating at different values of the gate voltage.

Our theoretical prediction of a reentrant insulator-to-metal-to-insulator transition and the reported gate voltage control calls for further experiments. Technical ap-

plications are discernible since these two control parameters should allow us to fine tune LCMO nanoclusters to the verge of a Mott transition. In this situation smallest changes in temperature, voltage, magnetic field etc. can trigger a gigantic change in conductance.

Acknowledgments

We acknowledge financial support from the Austrian Science Fund (FWF) through I-610-N16 (AV), the Deutsche Forschungsgemeinschaft FOR 1346 (GS), and the European Research Council under the European Union's Seventh Framework Program FP7/ERC through grant agreement n. 306447 (AV, KH) and n. 240524 (AV). HD and TSD would like to acknowledge Department of Science and Technology, India for the support. The numerical calculations were performed on the Vienna Scientific Cluster (VSC).

-
- ¹ G. M. Jonker and J. H. van Santen, *Physica* **16**, 337 (1950).
² R. von Helmolt, J. Wecker and B. Holzapfel and L. Schultz and K. Samwer *Phys. Rev. Lett.* **71**, 2331 (1993).
³ S. Jin, T. H. Tiefel, M. McCormack, R. A. Fastnacht, R. Ramesh, and L. H. Chen, *Science* **264**, 413 (1994).
⁴ R. M. Kusters, S. Singelton, D. A. Keen, R. McGreevy, and W. Hayes, *Physica B* **155**, 362 (1989).
⁵ P. Schiffer, A. P. Ramirez, W. Bao, and S-W. Cheong, *Phys. Rev. Lett.* **75**, 3336 (1995).
⁶ E. O. Wollan and W.C. Koehler, *Phys. Rev.* **100**, 545 (1955).
⁷ H. Kuwahara *et. al.*, *Science*, **270**, 961 (1995).
⁸ D. P. Kozlenko *et. al.*, *J. Phys. Cond. Mat.*, **16**, 5883 (2004).
⁹ A. Asamitsu *et. al.*, *Nature (London)*, **388**, 50 (1997).
¹⁰ T. Sarkar *et. al.*, *J Appl. Phys. Lett* **92**, 123104 (2008).
¹¹ T. Sarkar, B. Ghosh, A. K. Raychaudhuri, and T. Chatterji, *Phys.Rev. B* **77**, 235112 (2008).
¹² S. M. Zhou, S. Y. Zhao, Y. Q. Guo, J. Y. Zhao, and L. Shi, *J. Appl. Phys.* **107**, 033906 (2010).
¹³ P. M. Chowdhury *et al.*, *J. Nanopartical Research* **15**, 1585 (2013).
¹⁴ G. Iniyama *et al.*, *J. Appl. Phys.* **116**, 113901 (2014).
¹⁵ Z. Jirak *et al.*, *Phys. Rev. B* **81**, 024403 (2010).
¹⁶ S. S. Rao, S. Tripathi, D. Pandey, and S. V. Bhat, *Phys. Rev. B* **74** 144416 (2006).
¹⁷ K. S. Bhagyashree and S. V. Bhat, arXiv:1412.1450 (2014).
¹⁸ L. R. Goveas, K. N. Anuradha, K. S. Bhagyashree, and S. V. Bhat, *J. Appl. Phys.* **117**, 17E111 (2015).
¹⁹ T. Sarkar *et. al.*, *J. App. Phys.* **101** 124307 (2007).
²⁰ S. S. Rao *et. al.* *App. Phys. Lett*, **87**, 182503 (2005).
²¹ T. Zhang and M. Dressel, *Phys. Rev B* **80**, 014435 (2009).
²² H. Das, G. Sangiovanni, A. Valli, K. Held, and T. Saha-Dasgupta, *Phys. Rev. Lett.* **107**, 197202 (2011).
²³ See Supplemental Material at <http://link.aps.org/supplemental/10.1103/PhysRevLett.107.197202> for details on the crystal structures as well as on construction of the model structure.
²⁴ F.-L. Tang *et al* *J. Magn. Mag. Mater.* **333**, 8 (2013).
²⁵ C. Zener, *Phys. Rev.* **82**, 403 (1951).
²⁶ J. P. Perdew, K. Burke, M. Ernzerhof, *Phys. Rev. Lett.* **77**, 3865 (1996); J. P. Perdew, K. Burke, M. Ernzerhof, *Phys. Rev. Lett.* **78**, 1396 (1997).
²⁷ G. Kresse and J. Hafner, *Phys. Rev. B* **47**, 558 (1993).
²⁸ G. Kresse and J. Hafner, *Phys. Rev. B* **49**, 14251 (1994).
²⁹ G. Kresse and J. Furthmüller, *Comput. Mat. Sci.* **6**, 15 (1996).
³⁰ G. Kresse and J. Furthmüller, *Phys. Rev. B* **54**, 11169 (1996).
³¹ O. K. Andersen, *Phys. Rev. B* **12**, 3060 (1975).
³² O. K. Andersen and T. Saha-Dasgupta, *Phys. Rev. B* **62**, R16219 (2000).
³³ G. H. Wannier, *Phys. Rev.* **52**, 191 (1937).
³⁴ K. Held and D. Vollhardt, *Phys. Rev. Lett.* **84**, 5168 (2000).
³⁵ K. H. Ahn and A. J. Millis, *Phys. Rev. B* **61**, 13545 (2000).
³⁶ A. Yamasaki, M. Feldbacher, Y.-F. Yang, O. K. Andersen, and K. Held, *Phys. Rev. Lett.* **96**, 166401 (2006).
³⁷ This relation holds in the case of degenerate orbitals, with the Hamiltonian being invariant under orbital rotations. However, it is considered physically sensible also when the symmetry is fulfilled only approximately,³⁸ e.g., if the e_g orbitals are split by the Jahn-Teller crystal field.
³⁸ K. Held, *Advances in Physics* **56**, 829 (2007).
³⁹ J.-H. Park, C. T. Chen, S-W. Cheong, W. Bao, G. Meigs, V. Chakarian, and Y. U. Idzard, *Phys. Rev. Lett.* **76**, 4215 (1996).
⁴⁰ A. Flesch, E. Gorelov, E. Koch, and E. Pavarini, *Phys. Rev. B* **87**, 195141 (2013).
⁴¹ N. Parragh, A. Toschi, K. Held, and G. Sangiovanni, *Phys.*

- Rev. B **86**, 155158 (2012).
- ⁴² E. Gull, A. J. Millis, A. I. Lichtenstein, A. N. Rubtsov, M. Troyer, and P. Werner, Rev. Mod. Phys. **83**, 349 (2011).
- ⁴³ A. Georges, G. Kotliar, W. Krauth and M. Rozenberg, Rev. Mod. Phys. **68**, 13 (1996).
- ⁴⁴ M. Potthoff and W. Nolting, Phys. Rev. B **59**, 2549 (1999).
- ⁴⁵ M. Snoek, I. Titvinidze, C. Töke, K. Byczuk, and W. Hofstetter, New J. Phys. **10**, 093008 (2008).
- ⁴⁶ A. Valli, G. Sangiovanni, O. Gunnarsson, A. Toschi, and K. Held, Phys. Rev. Lett. **104**, 246402 (2010).
- ⁴⁷ A. Valli, G. Sangiovanni, A. Toschi, and K. Held, Phys. Rev. B **86**, 115418 (2012).
- ⁴⁸ I. Titvinidze, A. Schwabe, N. Rother, and M. Potthoff, Phys. Rev. B **86**, 075141 (2012).
- ⁴⁹ A. Valli, T. Schäfer, P. Thunström, G. Rohringer, S. Andergassen, G. Sangiovanni, K. Held, and A. Toschi, Phys. Rev. B **91**, 115115 (2015).
- ⁵⁰ Note that in general the Hund's exchange \mathcal{J} entails effective non-local (short-range) magnetic correlations between different Mn atoms, which are neglected in DMFT. However, it has been shown⁵¹ that those correlations are less important at high-temperature as well as for lattice structures with high-coordination, and DMFT provides reliable results. Also note that the average of an Ising spin $S = \pm 1$ yields the same DMFT Green function for the paramagnetic phase as the angular average of a classical spin with $|\vec{S}| = 1$.
- ⁵¹ D. Rotter, A. Valli, G. Sangiovanni, and K. Held, Eur. Phys. J. B, **86** (2013).
- ⁵² V. I. Anisimov, J. Zaanen, and O. K. Andersen, Phys. Rev. B **44**, 943 (1991).
- ⁵³ M. T. Czyżyk and G. A. Sawatzky, Phys. Rev. B **49**, 14211 (1994).
- ⁵⁴ J. E. Hirsch and R. M. Fye, Phys. Rev. Lett. **56**, 2521 (1986).
- ⁵⁵ L. Nordheim, Ann. Phys. (Leipzig) **9**, 607 (1931).
- ⁵⁶ A. Liebsch, Europhys. Lett. **63** 97 (2003).
- ⁵⁷ A. Koga, N. Kawakami, T. M. Rice and M. Sgrist, Phys. Rev. Lett. **92** 216402 (2004).
- ⁵⁸ R. Arita and K. Held, Phys. Rev. B **72** 201102(R) (2005).
- ⁵⁹ L. de Medici, A. Georges, and S. Biermann, Phys. Rev. B **72**, 205124 (2005).
- ⁶⁰ C. Knecht, N. Blümer, and P. G. J. van Dongen, Phys. Rev. B **72**, 081103(R) (2005).
- ⁶¹ E. Jakobi, N. Blümer, and P. G. J. van Dongen, Phys. Rev. B **80**, 115109 (2009); *ibid.* Phys. Rev. B **87**, 205135 (2013).
- ⁶² L. de' Medici, S. R. Hassan, M. Capone, and X. Dai, Phys. Rev. Lett. **102**, 126401 (2009).
- ⁶³ V. Anisimov, I. A. Nekrasov, D. E. Kondakov, T. M. Rice, and M. Sgrist, Eur. Phys. J. B **25**, 191 (2002).
- ⁶⁴ M. Neupane, P. Richard, Z.-H. Pan, Y.-M. Xu, R. Jin, D. Mandrus, X. Dai, Z. Fang, Z. Wang, and H. Ding, Phys. Rev. Lett. **103**, 097001 (2009).
- ⁶⁵ R. Yu and Q. Si, Phys. Rev. Lett. **110**, 146402 (2013).
- ⁶⁶ H. Park, A. J. Millis, and C. A. Marianetti, Phys. Rev. Lett. **109**, 156402 (2012).
- ⁶⁷ M. Karolak, M. Izquierdo, S. L. Molodtsov, and A. I. Lichtenstein, arXiv 1501.03294 (2015).